ORIGINAL PAPER

Investigation on influence of drilling unloading on wellbore stability in clay shale formation

Yi Ding[1,2] · Xiang-Jun Liu[1] · Ping-Ya Luo[1]

Abstract
Wellbore collapse frequently happens in the clay shale formation. To maintain wellbore stability, appropriate mud pressure is a vital factor. When clay formation is opened, drilling unloading occurs, modifying rock structure and strength at the wall of borehole, which affects the selection of mud pressure. Currently, mechanism of drilling unloading is still poorly understood which in return will bring a concern to wellbore stability. Therefore, in this study, a combination of triaxial compressive test and ultrasonic wave test has been used to simulate drilling unloading and analyze its mechanism. Results indicate that more void space is created inside the clay shale sample due to unloading. This structure change leads to a decline of strength and acoustic amplitude. Additionally, unloading influence is depended on varying drilling unloading parameters. Small unloading range and fast unloading rate are able to enhance stability. With various degrees of unloading impact, collapse pressure equivalent density has a clear modification, proving that unloading is a non-negligible influencing factor of wellbore stability. Besides, the unloading effect is much stronger in large confining pressure, implying that more attention should be given to unloading when drilling is in extreme deep or high geostress formation. Findings in this paper can offer theoretical guidance for drilling in the clay shale formation.

Keywords Drilling unloading · Clay shale · Wellbore stability · Rock strength

1 Introduction

Wellbore instability is a well-known problem in the drilling operation, causing huge economic loss (Chen et al. 2003; Rahman et al. 2000). In particular, clay shale has been considered as high-risk formation since numerous wellbore collapses occur (He et al. 2016; Wilson and Wilson 2014; Abdulhadi et al. 2012). Factors affecting wellbore stability in clay shale have been widely analyzed, including hydration, mechanical property, pore pressure, in situ stress, etc. For controlling clay shale hydration, chemical research has been carried out to produce efficient inhibitors and membrane-forming agents for drilling fluid (Zhong et al. 2016; Liu et al. 2014). Considering the influence of hydration on clay shale property, extensive hydration evaluation methods have been established (Tianshou and Chen 2014; Kang et al. 2017). Furthermore, wellbore collapse is the result of mechanical instability of rock, which raises large demands for research about rock mechanics. For instance, mechanical experiments, like triaxial, shear, tensile tests, have been applied to characterize the mechanical behavior of clay shale and find out appropriate strength criterion for the calculation of collapse pressure (Lai et al. 2007). Meanwhile, stress state of clay shale in subsurface has been discussed for wellbore stability. Studies from Han and Dusseault (2003), Roshan and Rahman (2011) and Abousleiman et al. (1997) show it is much easier for rock to have shear failure in formation with strong anisotropy and high value of in situ stress. Furthermore, because of the physicochemical reaction between clay shale and drilling fluid, pore pressure distribution around wellbore will be modified, affecting collapsing degree of borehole (Ghassemi et al. 2009). Correspondingly, based on Fick diffusion and Darcy law,

✉ Xiang-Jun Liu
liuxiangjunswpl@163.com

1   State Key Laboratory of Oil and Gas Reservoir Geology and Exploitation, Southwest Petroleum University, Chengdu 610500, Sichuan, People's Republic of China

2   Deep Earth Energy Lab, Department of Civil Engineering, Monash University, Melbourne 3800, Australia

models of pore pressure propagation have been built (Salehi et al. 2010).

The above statement gives so many influence factors of wellbore instability in clay shale formation, showing extreme complexity for this drilling problem. In oilfield, the most direct and effective method of maintaining well-bore stability is to choose appropriate mud pressure (Xia and Moore 2006). Generally, under the influence of drilling fluid on rock, mud pressure has to be adjusted with drilling time. Regarding mud pressure in the process of drilling, initial mud pressure is the foundation. If initial mud pressure is too low, wellbore collapse occurs immediately, forming irregular borehole shape and causing irreversible damage to rock around the wellbore (Ding et al. 2018). Under this circumstance, adjustment of mud pressure is not so useful, further elevating the challenge of keeping wellbore stability. When it comes to initial mud pressure, unloading influence cannot be avoided. Once formation is opened, drilling unloading happens immediately. There is no doubt that drilling unloading can cause damage to rock around wellbore. Hence, the selection of mud pressure should include this influence from unloading. However, current studies about wellbore stability do not cover the unloading effect, which is not beneficial for drilling in clay shale formation with high risk of wellbore collapsing.

Therefore, in this paper, we combine triaxial compressive test and ultrasonic wave test to simulate drilling unloading condition and to obtain rock strength and structure in the unloading process. Using these experimental data, we have analyzed the influence mechanism of unloading. Besides, influence factors of drilling unloading (unloading range, unloading rate and confining stress) have been investigated. The aim of this work is to illustrate the mechanism of drilling unloading. Outcomes of this paper can offer theoretical reference for drilling in clay shale formation.

2 Clay shale sample

In this study, mineral composition, clay composition and rock structure of clay shale have been presented by using XRD, visual observation and SEM (Fig. 1). Clay shale is composed by quartz, feldspar (orthoclase and plagioclase), carbonates (calcite and dolomite), clay and siderite. Meanwhile, clay consists of illite, smectite, I/S, kaolinite and chlorite. It is noted that clay is dominated in mineral composition and water-sensitive clay (smectite and I/S) is rich, suggesting strong hydration of clay shale. Strong hydration ability requires high standard for mud pressure in drilling. According to studies (Wang et al. 2006; Liu et al. 2009;
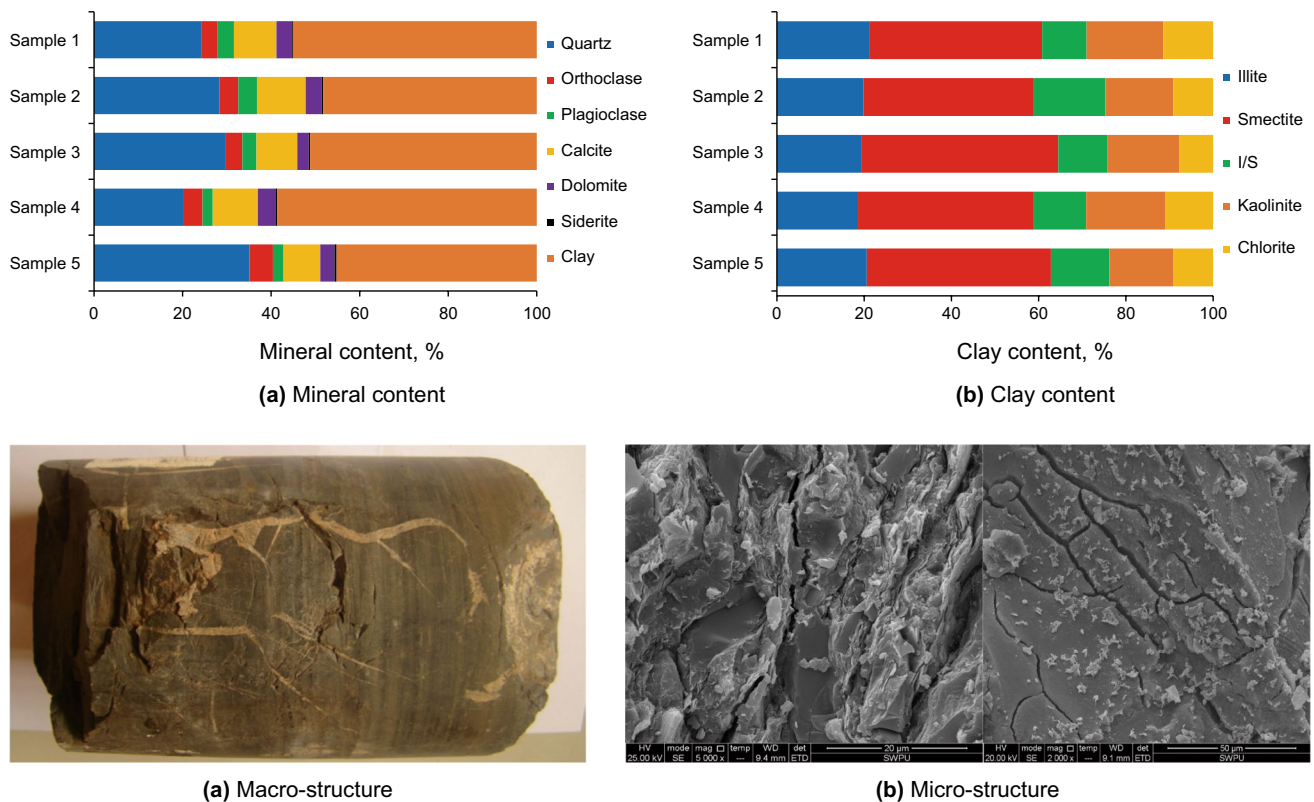

(a) Mineral content

(b) Clay content

(a) Macro-structure

(b) Micro-structure

Fig. 1 Rock composition and structure of clay shale

Riley et al. 2012; Abass et al. 2006), from research on Qigu, Kuqa, Marcellus and Khafji shale formation, all authors give the conclusion that hydration ability of clay shale is a significant factor of affecting wellbore stability.

Furthermore, structure of clay shale shows disintegration with obvious fractures in macro- and microscale (Fig. 1c, d). This characteristic results in strong mechanical instability of clay shale, which is one of the main reasons why wellbore collapse frequently happens. Meanwhile, clay shale has a relatively high sensitivity for external stress due to this mechanical instability (Cai et al. 2007; Zhu et al. 2018). In other words, with high degree of structure disintegration, it is much easier to cause rock failure. Particularly, in the beginning of drilling, when drilling fluid replaces rock, stress state around wellbore is suddenly changed from original stress balance condition to new stress state. If this new stress state is inappropriate, stronger compressive or tensile effect will be loaded on rock around wellbore. Consequently, structure disintegration of rock is aggravated, finally leading to rock failure. Therefore, initial mud pressure has to be precisely confirmed to establish balance of stress state on rock around wellbore.

3 Experimental method

3.1 Schematic of drilling unloading

When formation is opened by drilling, unloading effect is created. Take vertical borehole as an example; its schematic of drilling unloading is illustrated in Fig. 2. Before drilling, rock in formation is controlled by in situ stress. After drilling, rock in the borehole has been replaced by drilling fluid, making mud pressure support the wall of borehole. Stress state at the wall of borehole will be modified due to drilling unloading. At the direction along maximum and minimum horizontal stress (σ_H and σ_h), stresses are changed from σ_H and σ_h to mud pressure (σ_r), having $\sigma_H - \sigma_r$ and $\sigma_h - \sigma_r$ unloading range, respectively.

Stress state of rock at the wall of borehole can be simplified to two stresses, which are axial stress and lateral stress (Zhang et al. 2010). With the unloading effect, lateral stress is unloaded, decreasing its bracing impact on rock. As a result, axial stress has a relatively stronger compressive effect. Meanwhile, this increasing compressive effect is able to create more damage on rock structure, incurring crack initiation and propagation (Fig. 3). Since rock structure has been changed, rock mechanical property will have the corresponding modification, which is the main reason why drilling unloading can affect wellbore stability.

3.2 Simulation of drilling unloading

In order to simulate drilling unloading and analyze the mechanism of drilling unloading, triaxial compressive test and ultrasonic wave test have been combined, as shown in Fig. 4. In this experiment, placement of core sample is presented in Fig. 5. Besides, we use false triaxial condition ($\sigma_3 = \sigma_2$) and confining pressure is used to simulate drilling unloading. Confining pressure is firstly loaded. Hydraulic oil in tank is pushed by nitrogen gas pressure to fill the chamber. Once the chamber is full of oil, by using the control system of confining pressure, hydraulic power has been added into the chamber so that the confining pressure can be increased to a certain value. On the other hand, with the release of hydraulic power, decline of confining pressure can be finished. In a similar method, with axial pressure control system, hydraulic pressure can be added on pressure head to give axial load for core sample. Additionally, in the process of unloading test, ultrasonic source creates signal (P wave with 50 kHz), which goes through core sample from upper pressure head to lower pressure head. Finally, ultrasonic
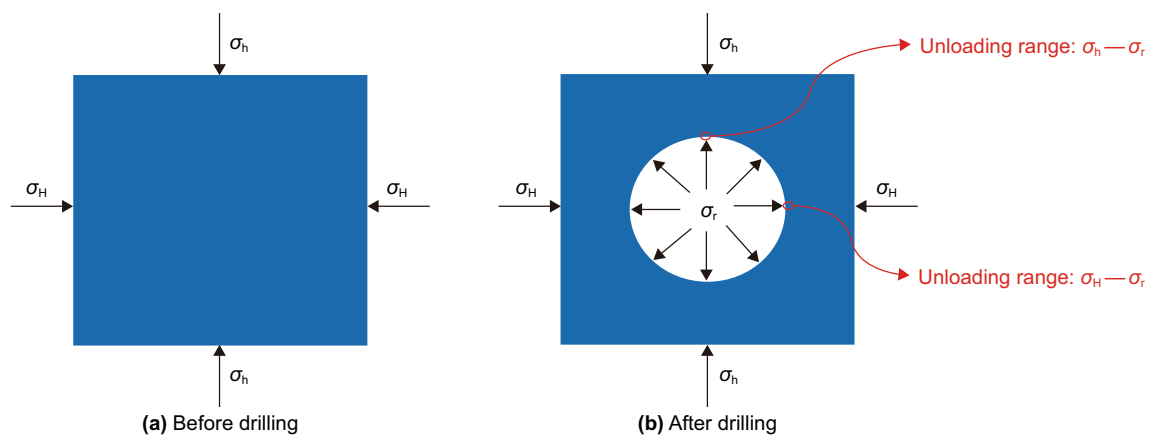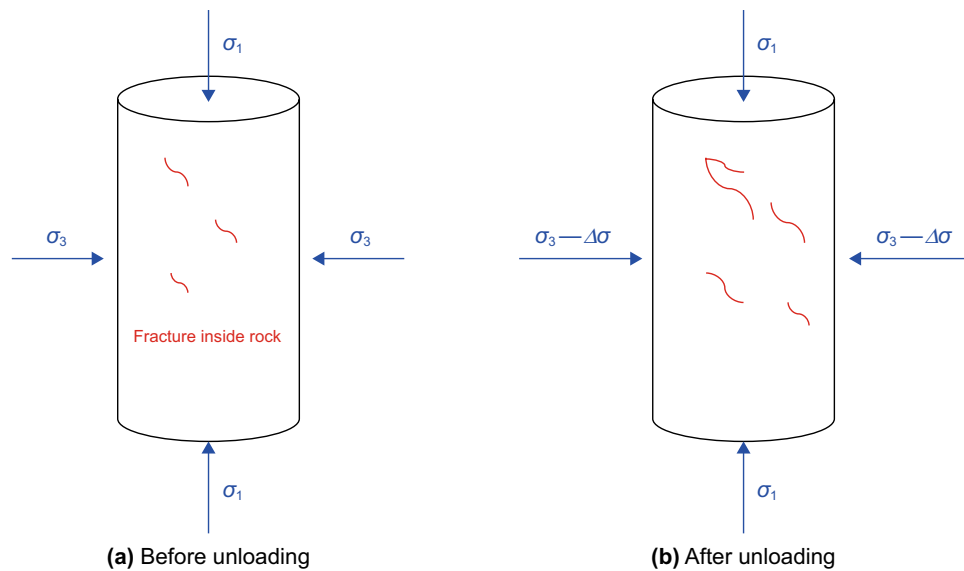

Fig. 2 Illustration of drilling unloading

(a) Before unloading   **(b)** After unloading

Fig. 3 Illustration of the unloading influence on rock

(1) Computer
(2) Ultrasonic source
(3) Oscilloscope
(4) Nitrogen cylinder
(5) Tank of hydraulic oil
(6) Flowmeter
(7) Load cell
(8) Upper pressure head
    with ultrasonic wave
(9) Lower pressure head
    with ultrasonic wave
(10) Axial strain gauge
(11) Core sample
(12) Pedestal
(13) Axial pressure
    control system
(14) Confining pressure
    control system
(15) Hydraulic power supply

Ultrasonic wave system

Fig. 4 Schematic of equipment with triaxial compressive test and ultrasonic wave test

signal after passing core sample is acquired in oscilloscope and acoustic data in unloading will be saved in computer.

The unloading condition is simulated by confining pressure in triaxial compressive test, and its stress path is shown in Fig. 6. In conventional triaxial test, confining pressure is firstly increased to a certain value. Subsequently, axial stress is increased until the rock sample has a failure (Fig. 6a). Based on this process, compressive strength in confining pressure can be acquired (Haimson and Chang 2000). To get the influence of unloading on

rock mechanical property, unloading phase has been added into the stress path, as shown in Fig. 6b. In the beginning, the step is the same as the conventional test, loading confining pressure to a certain value. After that, axial stress is increased to 80% of compressive strength (Point C). Then, with constant axial stress, the unloading phase starts, decreasing confining pressure from Point A to Point B. When the unloading process ends, axial stress restarts increasing until rock failure. Compared to conventional triaxial compressive test, unloading test has an unloading
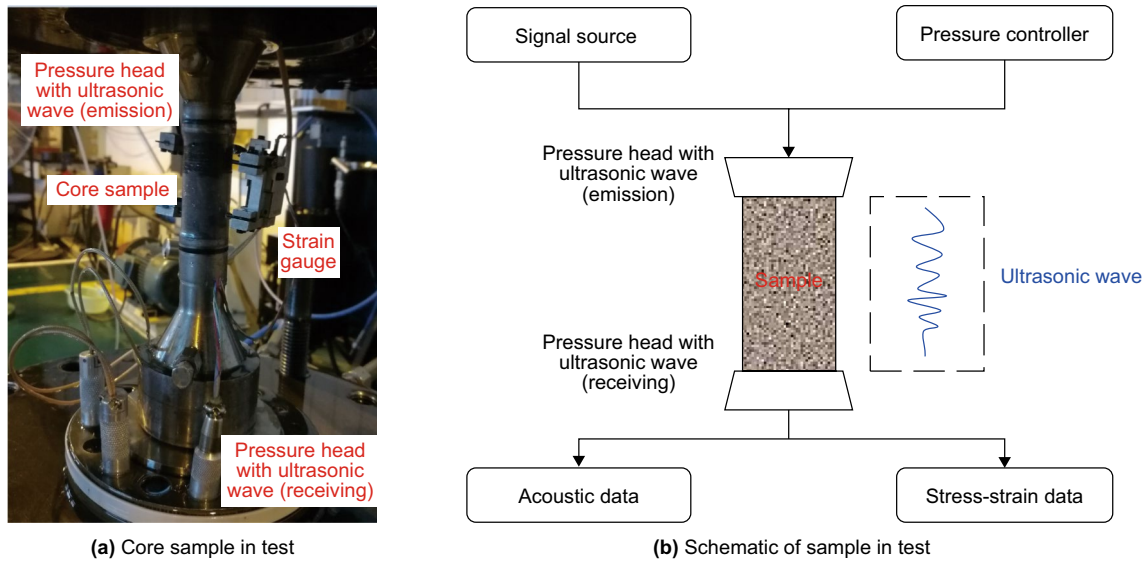
(a) Core sample in test

(b) Schematic of sample in test

Fig. 5 Illustration of core sample in test

(a) Conventional triaxial test
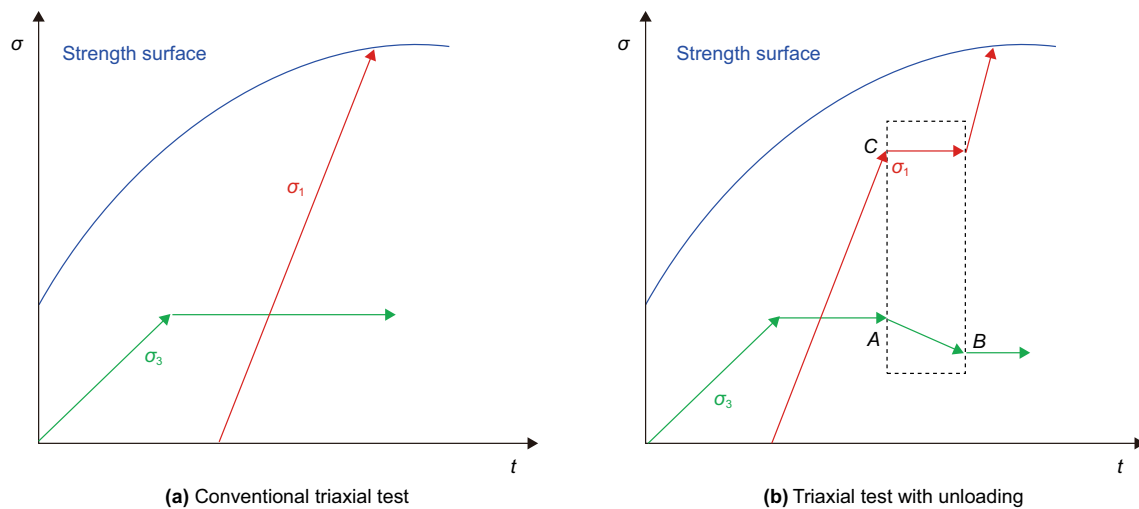
(b) Triaxial test with unloading

Fig. 6 Schematic of stress path in unloading simulation

phase, thus giving rock mechanical parameters containing the unloading effect.

In combination with conventional triaxial compressive test and triaxial ultrasonic test with unloading, experimental analysis of the influence of unloading on shale can be conducted. The whole experimental procedure is shown in Fig. 7. The experimental analysis is presented in the following section.

4 Experimental analysis

4.1 Rock strength with drilling unloading

Based on the triaxial compressive test with and without unloading, stress–strain curves are shown in Fig. 8.
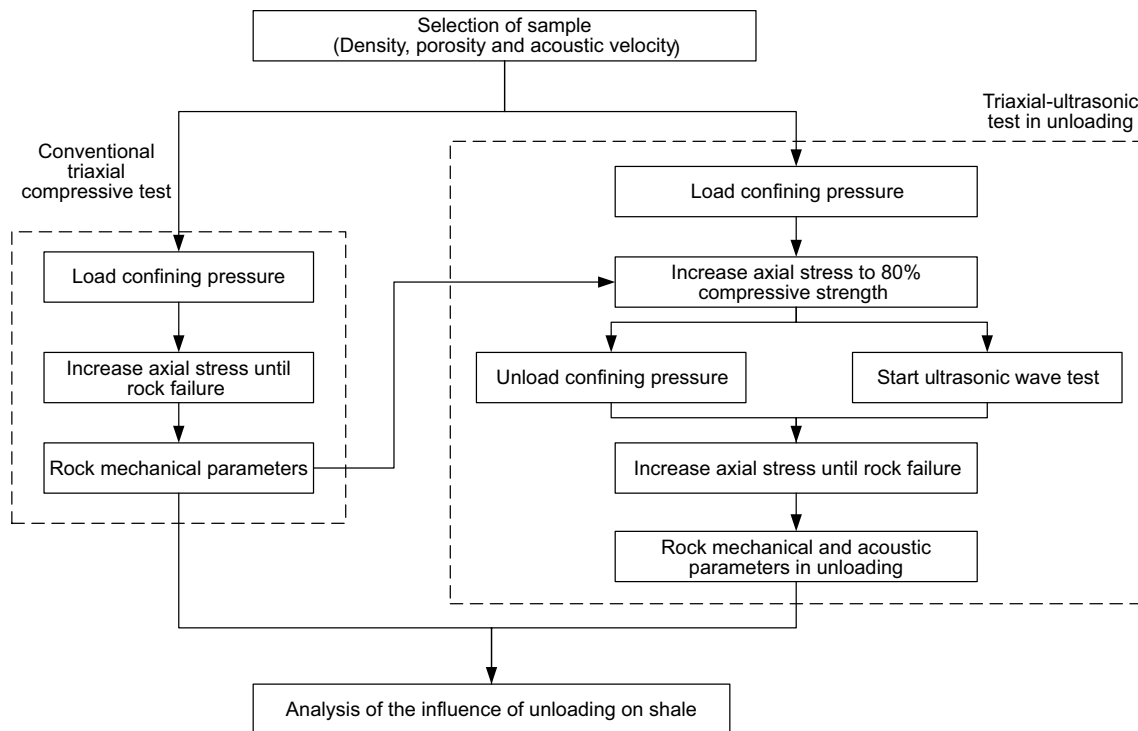
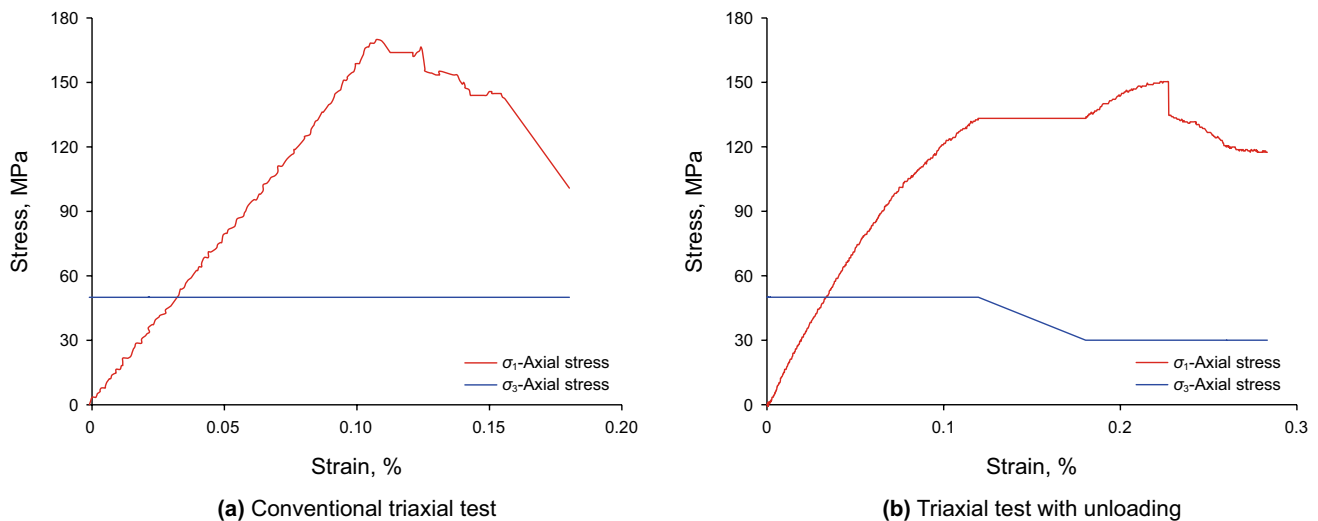**Fig. 7** Schematic of experimental analysis

Fig. 8 Stress–strain of triaxial compressive test in conventional and unloading

In unloading condition, stress–strain curve has flat line part, which is the unloading stage. Under certain unloading range, unloading process converts rock sample from one confined condition to another condition. Take unloading range = 20 MPa and confining pressure = 50 MPa as an example; confining pressure is changed from 50 to 30 MPa. Its compressive strength is located between strengths at 50 MPa and 30 MPa confining pressure, as shown in Fig. 9. Comparing to condition with $\sigma_3 = 50$ MPa, sample with unloading has smaller compressive strength due to damage caused by the unloading process. On the other hand, the strength of sample with unloading (σ_3 from 50 to 30 MPa) is relatively higher than compressive strength with $\sigma_3 = 30$ MPa. That is because sample

(a) Stress strain

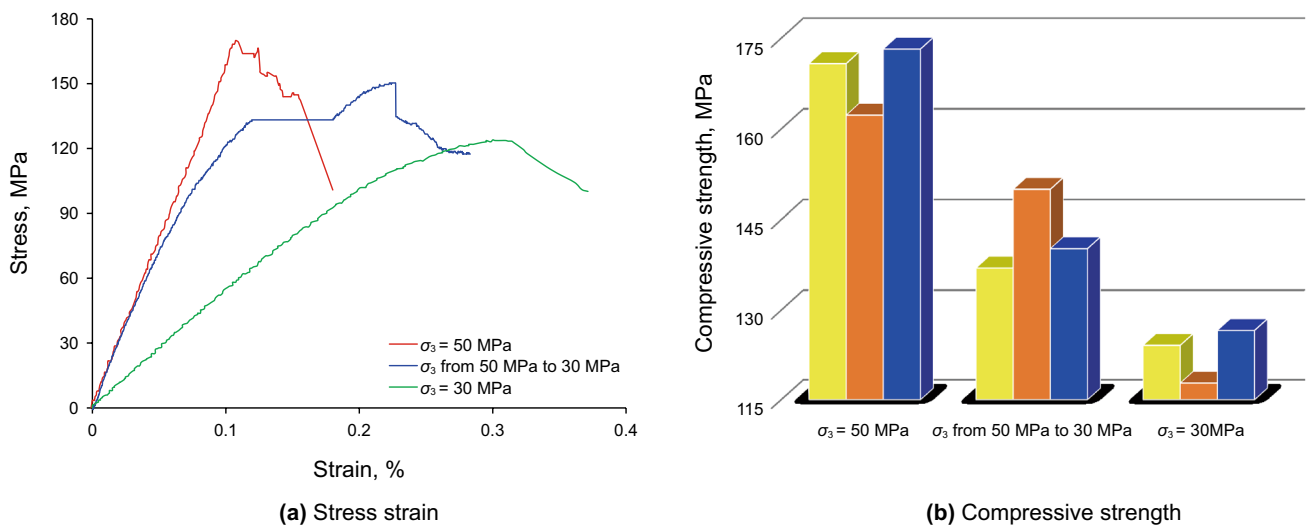**(b)** Compressive strength

Fig. 9 Comparison of strength property in conventional and unloading conditions

is unloaded from a higher confining pressure (50 MPa), which means a much stronger bracing effect exists before confining pressure decreases to 30 MPa, making relatively higher compressive strength.

In order to acquire mechanical parameters (cohesion and internal friction angle), we choose $\sigma_3^1 = 50$ MPa and $\sigma_3^2 = 30$ MPa to conduct triaxial compressive test in conventional and unloading conditions. The illustration of acquiring mechanical parameters in conventional and unloading conditions is presented in Fig. 10. As it is shown in Fig. 10, in conventional and unloading conditions, with certain confining pressures, triaxial compressive test is conducted to get stress–strain curves, respectively. Based on the compressive stress and confining stress, two Mohr's circles in conventional condition and two Mohr's circles in unloading condition have been formed. By using these Mohr's circles, Mohr–Coulomb criterion has been applied to acquire mechanical parameters in conventional and unloading conditions, as follows:

$$\begin{cases} \varepsilon = c + \sigma \tan \varphi & \text{(In conventional condition)} \\ \varepsilon = c_u + \sigma \tan \varphi_u & \text{(In unloading condition)} \end{cases} \quad (1)$$

where ε and σ are shear and normal stresses at failure plane, MPa; c and c_u are cohesion in conventional and unloading conditions, respectively, MPa; φ and φ_u are internal friction angle in conventional and unloading conditions, respectively, degree.

4.2 Acoustic property in unloading

Acoustic property can reflect the structure of core sample. Based on that, in the unloading, ultrasonic wave test has

been conducted to obtain the acoustic property of core sample, as shown in Fig. 11. For the unloading process, ultrasonic waves in the beginning and ending point (i.e., point A and B in Fig. 11a) have been acquired, respectively. It is well known that acoustic amplitude can be considered as a signal of acoustic energy (Xu et al. 2019, 2017). Besides, the development of void space (fracture or porosity) increases the number of acoustic reflections, refraction and scattering in ultrasonic wave propagation inside rock. Consequently, more acoustic energies have been absorbed in this propagation, leading to a small amplitude. Therefore, acoustic amplitude represents the evolutionary process of rock structure in unloading (Weger et al. 2009). Figure 11b shows the acoustic amplitude in unloading, showing that the amplitude has a decline after unloading, which indicates that structure damage is gradually increased and more void space is produced in unloading.

4.3 Structure of clay shale in unloading

Maximum amplitude (i.e., maximum absolute value of acoustic amplitude) is the typical feature of acoustic amplitude and can represent acoustic energy (Zou et al. 2017). Considering the relation between rock structure and acoustic amplitude, in this section, we use maximum amplitude to be an indicator of structural damage degree under external stress impact, establishing quantitative method of rock structural damage. For intact core sample of clay shale, its void space is located at small range, which is not sufficient to reflect structural change from external stress. Hence, we add variable loadings on sample to create different degrees of structure damage. Axial loadings are equal to 0% (intact sample), 30%, 60%, 90% and 100% (sample after failure)
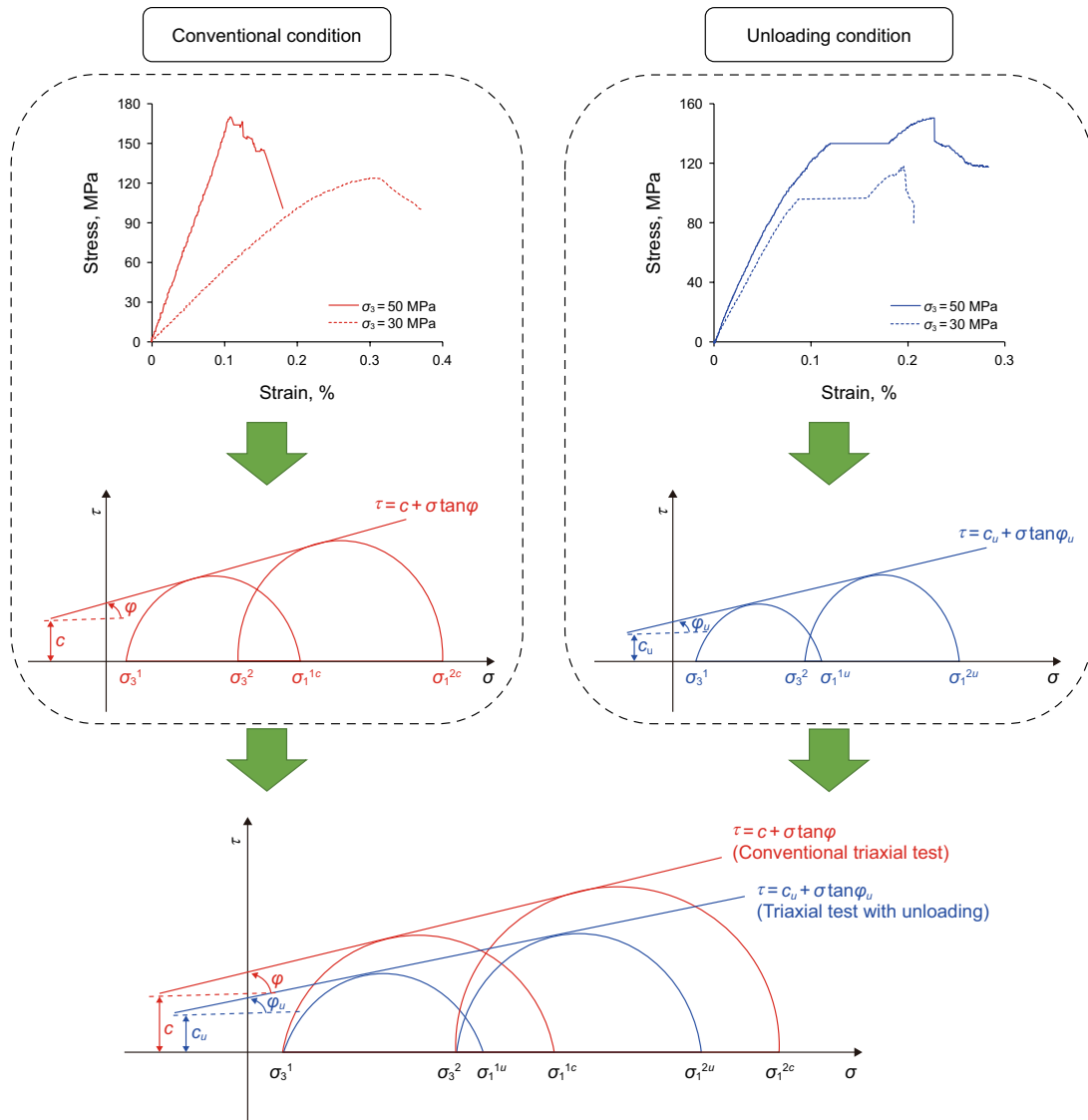
Fig. 10 Mohr's circle with and without drilling unloading

of uniaxial compressive strength (UCS). After the uniaxial loading process, porosity test and ultrasonic wave test of rock sample have been performed to acquire quantitative relation between acoustic amplitude and rock structure, as shown in Fig. 12. Its equation is given as Eq. (2). It can be found that with increasing void space (larger structure damage), acoustic maximum amplitude shows a decline, which is consistent with the theory of acoustic energy attenuation. Before 60% of UCS, increasing rate of void space is relatively slow. After that, the structural damage dramatically increases.

$$S_p = 39.476 \cdot e^{-0.004 \cdot A_m} \tag{2}$$

where S_p is the void space, %, and A_m is the P wave maximum acoustic amplitude, mV.

Unloading is one of the stress state modifications. When the stress state of rock is changing, the corresponding change in rock structure (crack initiation and propagation, open and closure of pore and crack, etc.) will occur (Liu et al. 2006). Based on the maximum amplitude before and after drilling unloading, acoustic amplitude can be used to express structure damage. Therefore, in this paper, structure damage of unloading can be evaluated using ultrasonic wave test in the unloading stage, as follows:

$$\Delta S_p = S_p^1 - S_p^o = 39.476 \cdot (e^{-0.004 \cdot A_m^1} - e^{-0.004 \cdot A_m^o}) \tag{3}$$
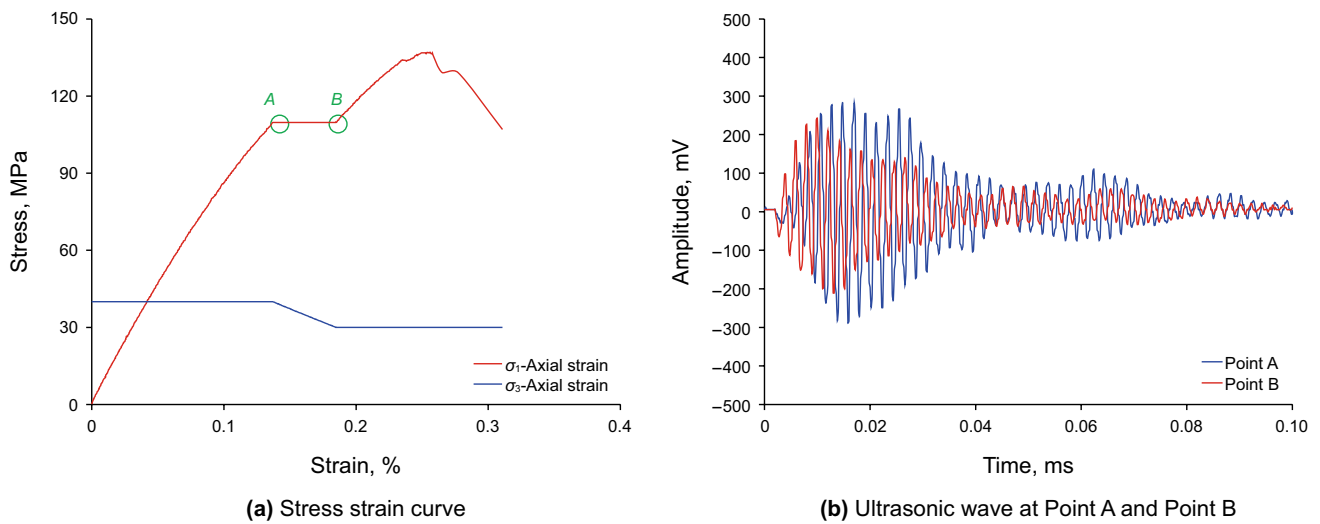
(a) Stress strain curve

(b) Ultrasonic wave at Point A and Point B

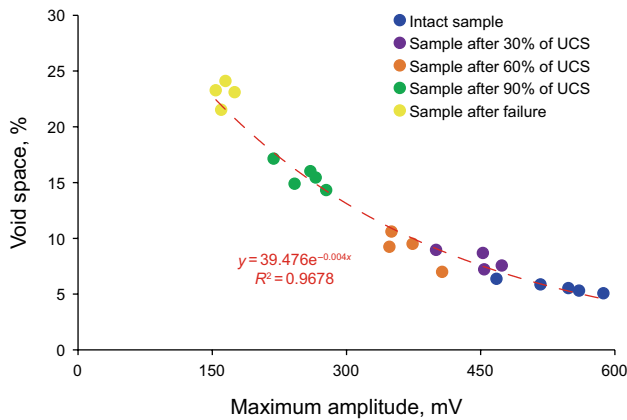**Fig. 11** Ultrasonic wave in unloading stage

Fig. 12 Different structural damage of core sample

where ΔS_p is the increment of void space after unloading, %; S_p^o is the void space in the beginning of unloading, %; S_p^1 is the void space in the ending of unloading, %; A_m^o is the maximum acoustic amplitude in the beginning of unloading, mV; A_m^1 is the maximum acoustic amplitude in the ending of unloading, mV.

5 Results and discussion

5.1 Influence of unloading range

In drilling operation, with variable mud pressure, in situ stress and well trajectory, different unloading ranges can be formed (Gholami et al. 2015). To investigate the influence of unloading range, unloading test has been conducted with different unloading ranges. In this test, loading and

Table 1 Testing parameters for samples with different unloading ranges

No.	Unloading range, MPa	Unloading rate, MPa s^1	Confining pressure, MPa	Axial stress, MPa
1	0	0.2	50	135
2	10	0.2	50	135
3	15	0.2	50	135
4	20	0.2	50	135
5	25	0.2	50	135
6	0	0.2	30	98.2
7	10	0.2	30	98.2
8	15	0.2	30	98.2
9	20	0.2	30	98.2
10	25	0.2	30	98.2

unloading rates are both 0.2 MPa/s. The confining pressures are 50 MPa and 30 MPa, as given in Table 1. Based on this test, rock strength parameters in different unloading ranges are shown in Fig. 13. Cohesion and internal friction angle both show clear decreasing tendency, indicating that large unloading range has a strong decline of rock strength. Meanwhile, at $\sigma_3 = 50$ MPa, according to acoustic maximum amplitude in the beginning and ending of unloading, increment of void space with different unloading ranges (σ_u) has been obtained, as shown in Fig. 14. It can be found out that high unloading range represents large increment of void space, having stronger attenuation of acoustic amplitude and larger structure damage caused by unloading.

The reason of larger structural damage in high unloading range is that increasing unloading range leads to the growth of axial differential stress ($\sigma_1 - \sigma_3$), which can have
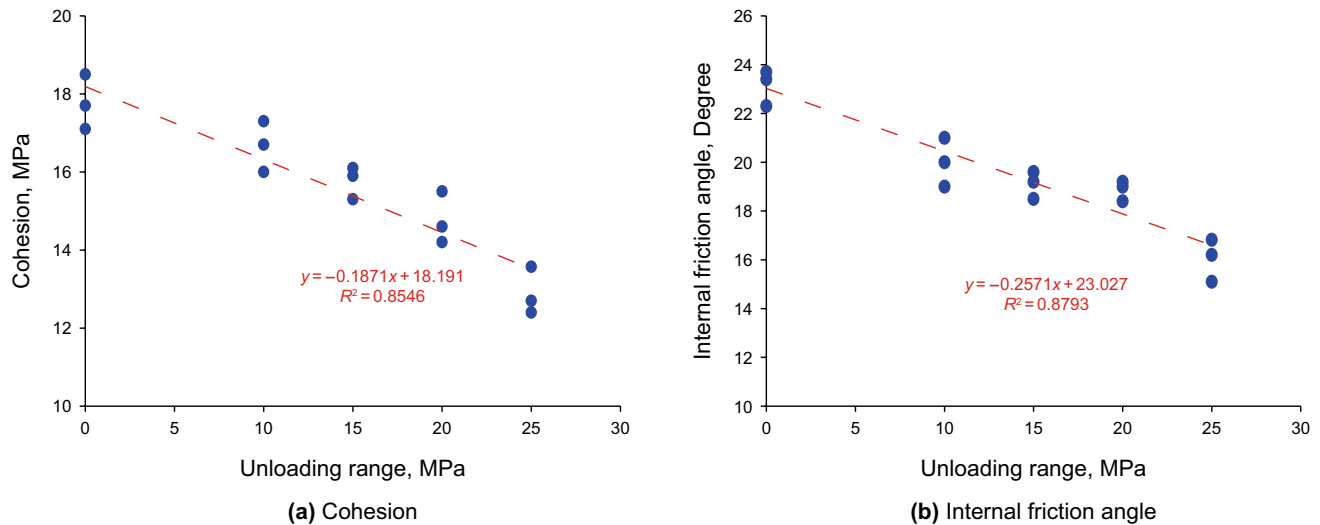
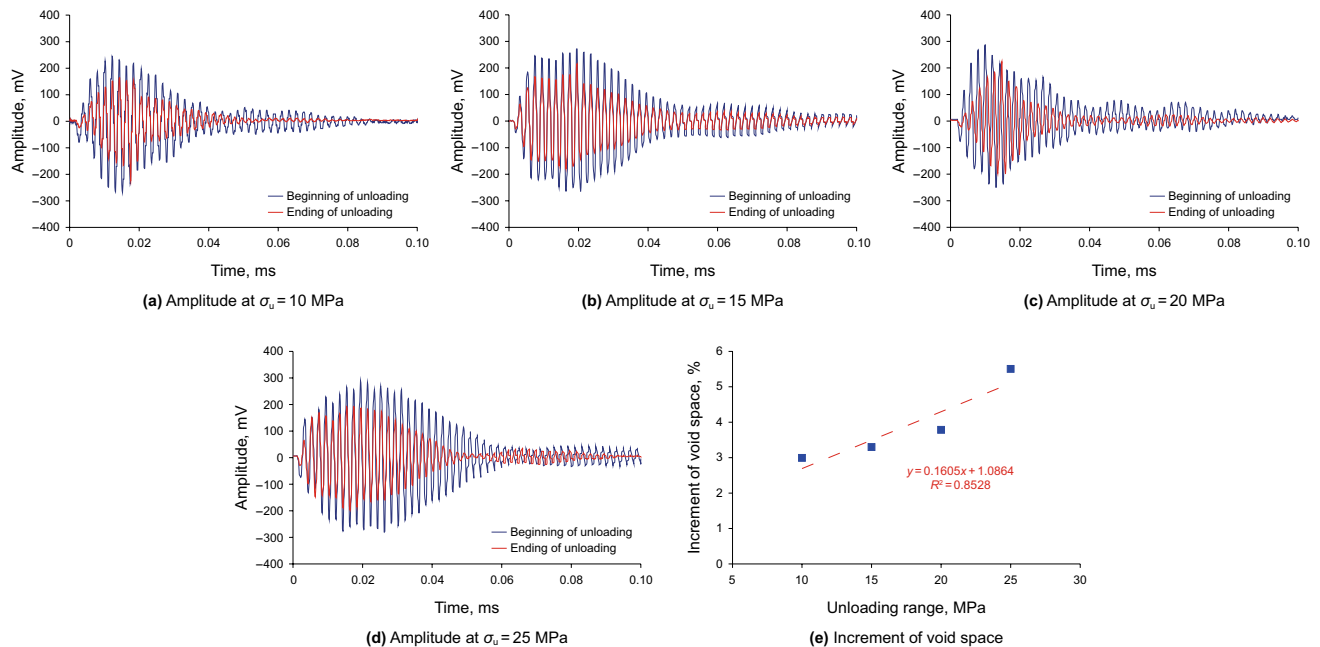**Fig. 13** Rock strength with unloading range

Fig. 14 Acoustic amplitude and void space with unloading range

a stronger compressive effect along the axial direction. In this case, more damage is created under large differential stress, causing increment of void space. As a result, rock strength shows a larger decline and clay shale becomes more unstable, elevating the risk of wellbore collapse in drilling.

5.2 Influence of unloading rate

Drilling rate is an important parameter in drilling operation. Fast drilling rate means formation is open in high speed,

having a large unloading rate. In this section, with different unloading rates, unloading test has been applied to investigate the influence of unloading rate on core sample. In this test, unloading range stays 20 MPa and confining pressures are 50 MPa and 30 MPa, as given in Table 2. The results are illustrated in Figs. 15 and 16. It is shown that with increasing unloading rate, rock strength rises, indicating that a fast drilling rate can enhance the wellbore stability. Correspondingly, at high speed of unloading, acoustic amplitude increases and void space decreases, meaning small structure damage in the

Table 2 Testing parameters for samples with different unloading rates

No.	Unloading range, MPa	Unloading rate, MPa s^{-1}	Confining pressure, MPa	Axial stress, MPa
1	20	0.2	50	135
2	20	0.6	50	135
3	20	1.0	50	135
4	20	1.6	50	135
5	20	2.0	50	135
6	20	0.2	30	98.2
7	20	0.6	30	98.2
8	20	1.0	30	98.2
9	20	1.6	30	98.2
10	20	2.0	30	98.2

unloading stage. The tendency of strength parameters with the unloading rate is typical *S* curves, expressed as

$$\begin{cases} c_u = \dfrac{4.3}{1+170.2\cdot e^{-5.1\cdot V_u}} + 14.7 \\ \varphi_u = \dfrac{3.9}{1+184.2\cdot e^{-4.4\cdot V_u}} + 18.7 \end{cases} \quad (4)$$

where V_u is the unloading rate, MPa/s.

The central reason for better stability in fast rate is stress lag phenomenon. The stress lag is normally noticed in the viscoelasticity medium. With a large content of clay, clay shale can be treated as the viscoelasticity medium (Arash et al. 2018). Due to the property of viscoelasticity, stress inside rock normally lags behind stress outside rock, creating lag stress between stress inside and outside of core sample, as shown in Fig. 17. The stress outside rock is equal to the sum of stress inside rock and lag stress (Fig. 17a).

For certain point inside sample (Point B in Fig. 17a), when unloading happens, small unloading rate gives more time for outside stress to go into rock, which makes stress path of Point B much closer to outside stress. Consequently, comparatively smaller lag stress ($\sigma_u - \sigma_u^1$) exists. On the other hand, if the unloading rate is fast, stress inside rock (Point B) does not have enough time to have the corresponding reaction with outside stress, showing larger lag stress ($\sigma_f - \sigma_f^2$). That is to say, with certain unloading range from outside, rock interior has small stress in high unloading rate ($\sigma_f^1 < \sigma_u^1$), indicating that rock interior has small damage. That is the reason why sample shows small change in acoustic amplitude and high-strength parameters in fast unloading rate.

Furthermore, when unloading rate is extremely small, outside stress can be passed through core sample and inside stress has plenty of time to modify with outside stress, causing lag stress negligible ($\sigma_u \approx \sigma_u^1$). In contrast, when unloading is fast enough, inside stress barely has to respond to outside stress ($\sigma_f^1 \approx 0$ MPa), thus leading the lag stress to reach a maximum value. Due to limiting value of lag stress, rock strength, acoustic amplitude and void space all exhibit *S*-type curve (Figs. 15, 16f), having obvious boundary at low and high unloading rates.

5.3 Influence of confining pressure in unloading

In drilling operation, rock at the wall of borehole is under confined stress condition (Sayers et al. 2009). Because of different in situ stress circumstances, confining pressure is variable. Considering different confining pressures, the unloading effect has been analyzed in this section. It is well known that compressive strength can be used to evaluate
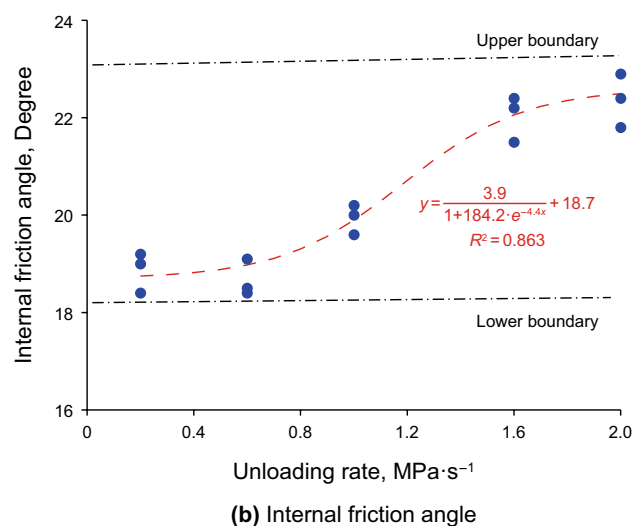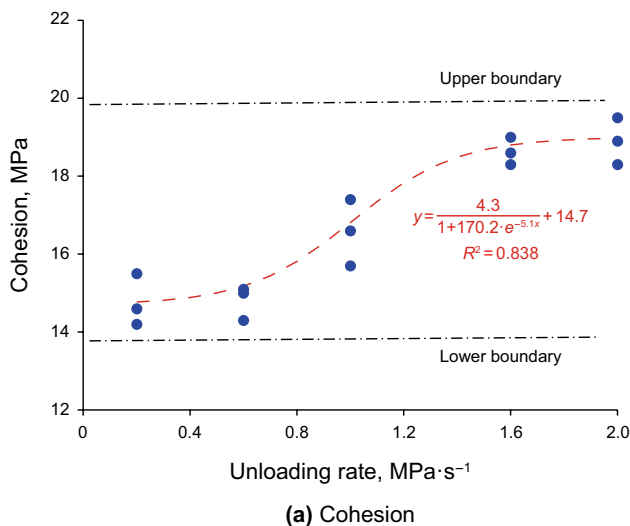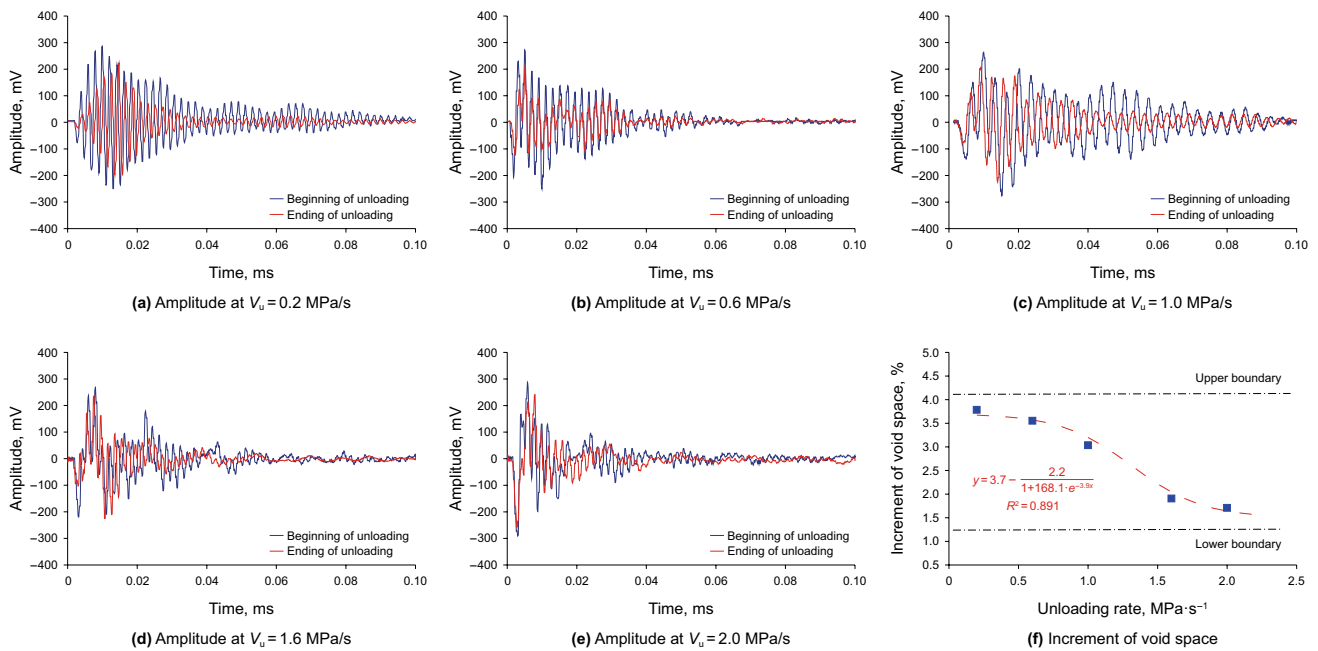

Fig. 15 Rock strength with unloading rate

(a) Amplitude at $V_u = 0.2$ MPa/s

(b) Amplitude at $V_u = 0.6$ MPa/s

(c) Amplitude at $V_u = 1.0$ MPa/s

(d) Amplitude at $V_u = 1.6$ MPa/s

(e) Amplitude at $V_u = 2.0$ MPa/s

(f) Increment of void space

Fig. 16 Acoustic amplitude and void space with unloading rate

(a) Illustration of inside and outside stress

(b) Lag stress with variable unloading rates
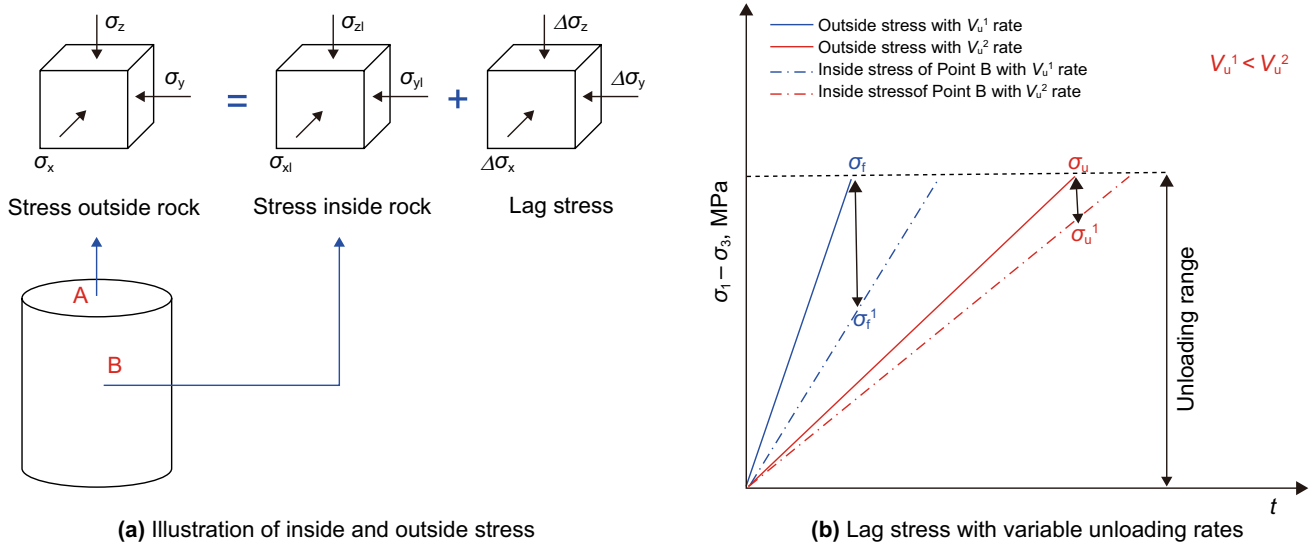
Fig. 17 Schematic of stress lag for rock

rock strength and stability (Ashour 1988). Thus, we use compressive strength to analyze unloading influence with different confining pressures. First of all, in conventional condition, compressive strength with different confining pressures has been acquired, as shown in Fig. 18. Same as previous researches (Takahashi 2012), experimental results illustrate linear relation between compressive strength and confining pressure. Since compressive strength is associated with confining pressure, to purely see the influence of confining pressure on unloading, each sample is given the

same state, meaning the same unloading parameters except confining pressure, as shown in Table 3.

With different confining pressures, unloading influence is presented in Figs. 19 and Fig. 20. It is clearly seen that the strength difference between the conventional test and unloading test grows with confining pressure. In 10 MPa confining pressure, the difference of compressive strength ($\Delta\sigma_c$) is merely 6.8 MPa. When confining stress reaches 50 MPa, difference has become approximately 18.8 MPa. Meanwhile, with increasing confining pressure, structural
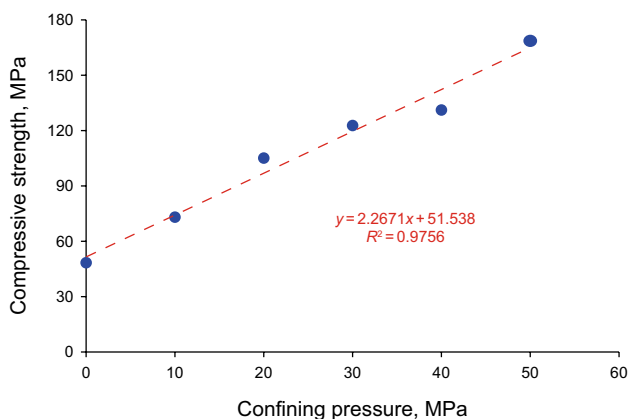
Fig. 18 Compressive strength with different confining pressures

Table 3 Testing parameters for samples with different confining pressures

No.	Unloading range, MPa	Unloading rate, MPa s^1	Confining pressure, MPa	Axial stress, MPa
1	10	0.2	10	58.5
2	10	0.2	20	84.1
3	10	0.2	30	98.2
4	10	0.2	40	105.0
5	10	0.2	50	135.0
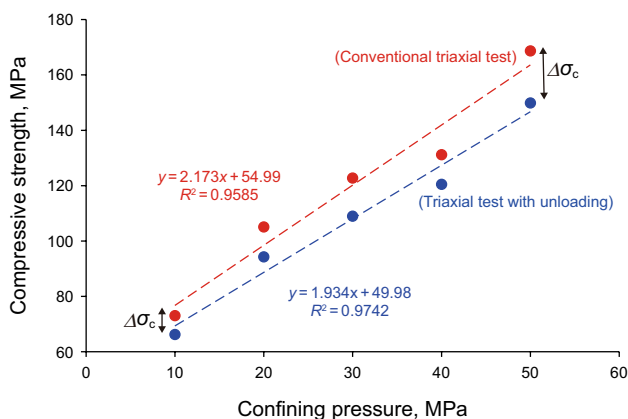
Fig. 19 Compressive strength in unloading with different confining pressures

damage and acoustic amplitude attenuation made from unloading are becoming large. These phenomena indicate that unloading influence is stronger in extreme deep formation or high geostress formation. Thus, drilling unloading should be given more attention when drilling operation is performed in these geological conditions.

5.4 Influence of unloading on collapse pressure

In order to clarify the influence of unloading in application, based on experimental analysis from the above sections, take vertical well as a case, we conduct the calculation of collapse pressure considering the influence of unloading. In this calculation, we assume that depth is constant ($H = 2930$ m) and set three typical in situ stress conditions, which are normal fault ($\sigma_v > \sigma_H > \sigma_h$), reverse fault ($\sigma_H > \sigma_h > \sigma_v$) and strike-slip fault ($\sigma_H > \sigma_v > \sigma_h$), as shown in Table 4. Besides, pore pressure is constant ($p_p = 32.1$ MPa) and all rock mechanical parameters are acquired from the above experiments.

For vertical wellbore, stress distribution at the wall of borehole can be calculated (Lee et al. 2012):

$$\begin{cases} \sigma_r = p_i - \phi(p_i - p_p) \\ \sigma_\theta = -p_i + (1 - 2\cos 2\theta)\sigma_H + (1 + 2\cos 2\theta)\sigma_h + K(p_i - p_p) \\ \sigma_z = \sigma_v + 2v(\sigma_H - \sigma_h) + K(p_i - p_p) \\ \tau_{z\theta} = 0 \\ K = \frac{a(1-2v)}{1-v} - \phi \end{cases}$$ (5)

where σ_r, σ_θ and σ_z are the radial, hoop and axial stress in wellbore coordinates, respectively, MPa; $\tau_{z\theta}$ is the component of shear stress in wellbore coordinates, MPa; p_p is the pore pressure, MPa; ϕ is the porosity, %; a is the Biot coefficient; v is the Poisson ratio; and θ is the wellbore circumferential angle, degree.

Based on the stress distribution in Eq. (5), principal stresses (σ_i, σ_j, σ_k) can be acquired by using Eq. (6). By conducting comparison among all principal stresses, maximum and minimum principal stresses can be determined. Subsequently, with maximum and minimum principal stresses, Mohr–Coulomb criterion can be applied to acquire collapse pressure.

$$\begin{cases} \sigma_i = p_i - \phi(p_i - p_p) \\ \sigma_j = \frac{\sigma_z - \sigma_\theta}{2} + \sqrt{\left(\frac{\sigma_\theta - \sigma_z}{2}\right)^2 + \tau_{z\theta}^2} \\ \sigma_k = \frac{\sigma_z - \sigma_\theta}{2} - \sqrt{\left(\frac{\sigma_\theta - \sigma_z}{2}\right)^2 + \tau_{z\theta}^2} \end{cases}$$ (6)

Considering the varying influence of unloading on rock strength, collapse pressure equivalent density is presented in Fig. 21. Collapse pressure equivalent density shows increment with rising unloading range. Meanwhile, too low unloading rate is detrimental for wellbore stability. These results indicate that drilling parameters are related to influencing degree of unloading. Appropriate mud pressure and drilling rate are vital for controlling unloading damage on wellbore stability. Thus, when it comes to prediction of collapse pressure, the unloading effect is non-negligible.
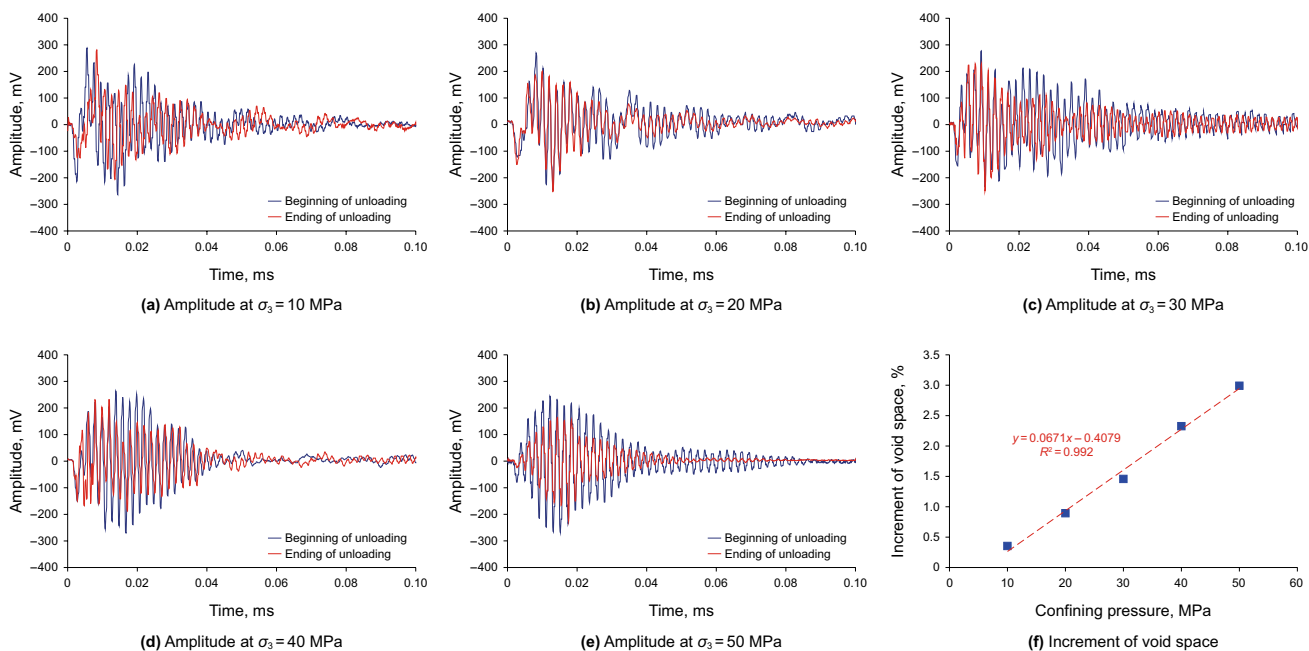
Fig. 20 Acoustic amplitude and void space in unloading with different confining pressures

Table 4 In situ stress distribution

No.	σ_v, MPa	σ_H, MPa	σ_h, MPa
1	62.3	56.4	51.2
2	51.2	62.3	56.4
3	56.4	62.3	51.2

6 Conclusion

In this study, to better control wellbore stability, drilling unloading has been simulated and its effect mechanism on rock stability has been discussed. The following conclusions are drawn:

1. A new experiment combining triaxial compressive test and ultrasonic wave test has been designed to simulate drilling unloading and obtain the influence of drilling
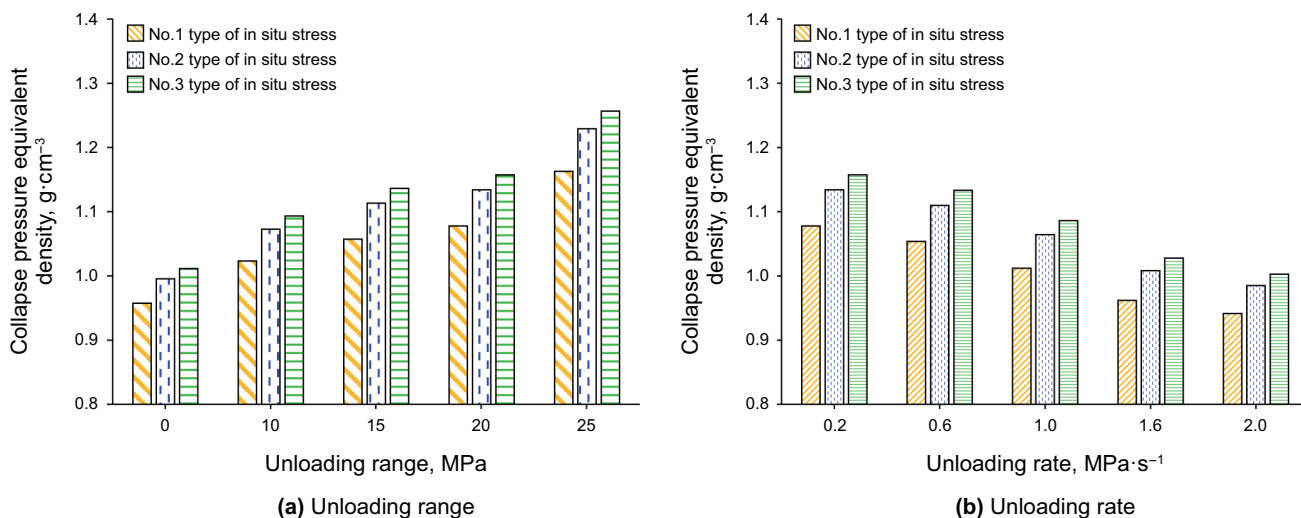
Fig. 21 Influence of unloading on collapse pressure equivalent density

unloading. In the unloading stage, rock acoustic amplitude shows a decline, suggesting that structure damage has been done by unloading. Furthermore, because of this damage in the unloading stage, rock strength (cohesion and internal friction angle) after unloading is clearly lower than rock sample without unloading, indicating that unloading can cause strength decline and increase rock mechanical instability.

2. High unloading range tends to have relatively large strength decline for clay shale. This is because large unloading of confining pressure decreases the lateral bracing effect on rock, thus causing a comparatively stronger compressive effect on rock. As a result, stronger damage and bigger strength decline are made. In addition, with increasing unloading rate, rock strength rises, suggesting that fast drilling rate can enhance wellbore stability. Meanwhile, at high speed of unloading, acoustic amplitude increases and void space decreases, meaning small structure damage in unloading. The stress lag is the reason of stronger stability in high speed of unloading. Under large unloading rate, inside stress cannot have immediate reaction for outside stress, which makes less damage inside rock and has smaller strength decline.

3. With increasing confining pressure, the damage made from unloading is becoming large. For certain drilling unloading parameters, decline of compressive strength is large in high confining pressure. Besides, void space is increasing with confining pressure. These phenomena demonstrate that unloading influence is stronger in extreme deep formation or high geostress formation. Thus, drilling unloading is non-negligible when drilling operation is conducted in these geological conditions.

References

Abass H, Shebatalhamd A, Khan M, Al-Shobaili Y, Ansari A, Ali S, Mehta S. Wellbore instability of shale formation; Zuluf field, Saudi Arabia. In: SPE technical symposium of saudi arabia section, 21–23 May, Dhahran, Saudi Arabia; 2006. https://doi.org/10.2118/106345-MS

Abdulhadi NO, Germaine JT, Whittle AJ. Stress-dependent behavior of saturated clay. Can Geotech J. 2012;49(8):907–16. https://doi.org/10.1139/t2012-057.

Abousleiman Y, Cui L, Ekbote S, Zaman M, Roegiers JC, Cheng AHD. Applications of time-dependent pseudo-3D stress analysis in evaluating wellbore stability. Int J Rock Mech Min Sci. 1997;34(3):10–211. https://doi.org/10.1016/S1365-1609(97)00207-4.

Ashour H. A compressive strength criterion for anisotropic rock materials. Can Geotech J. 1988;25(2):233–7. https://doi.org/10.1139/t88-027.

Arash KA, Ehsan G, Pania N, Mathew S. Elastic, viscoelastic, and strength properties of Marcellus Shale specimens. J Pet Sci Eng. 2018;171:662–79. https://doi.org/10.1016/j.petrol.2018.05.074.

Cai M, Kaiser PK, Tasaka Y, Minami M. Determination of residual strength parameters of jointed rock masses using the GSI system. Int J Rock Mech Min Sci. 2007;44(2):247–65. https://doi.org/10.1016/j.ijrmms.2006.07.005.

Chen G, Chenevert ME, Sharma MM, Yu M. A study of wellbore stability in shales including poroelastic, chemical, and thermal effects. J Pet Sci Eng. 2003;38(3–4):167–76. https://doi.org/10.1016/S0920-4105(03)00030-5.

Ding Y, Luo P, Liu X, Liang L. Wellbore stability model for horizontal wells in shale formations with multiple planes of weakness. J Nat Gas Sci Eng. 2018;52:334–47. https://doi.org/10.1016/j.jngse.2018.01.029.

Ghassemi A, Tao Q, Diek A. Influence of coupled chemo-poro-thermoelastic processes on pore pressure and stress distributions around a wellbore in swelling shale. J Pet Sci Eng. 2009;67(1–2):57–64. https://doi.org/10.1016/j.petrol.2009.02.015.

Gholami R, Rasouli V, Aadnoy B, Mohammadi R. Application of in situ stress estimation methods in wellbore stability analysis under isotropic and anisotropic conditions. J Geophys Eng. 2015;12(4):657–73. https://doi.org/10.1088/1742-2132/12/4/657.

Han G, Dusseault MB. Description of fluid flow around a wellbore with stress-dependent porosity and permeability. J Pet Sci Eng. 2003;40(1):1–16. https://doi.org/10.1016/S0920-4105(03)00047-0.

Haimson BC, Chang C. A new true triaxial cell for testing mechanical properties of rock, and its use to determine rock strength and deformability of Westerly granite. Int J Rock Mech Min Sci. 2000;37(1):285–96. https://doi.org/10.1016/S1365-1609(99)00106-9.

He S, Liang L, Zeng Y, Yi D, Lin Y, Liu X. The influence of water-based drilling fluid on mechanical property of shale and the wellbore stability. Petroleum. 2016;2(1):61–6. https://doi.org/10.1016/j.petlm.2015.12.002.

Kang Y, Yang B, Li X, Yang J, You L, Chen Q. Quantitative characterization of micro forces in shale hydration and field applications. Pet Explor Dev. 2017;44(2):328–35. https://doi.org/10.1016/S1876-3804(17)30038-1.

Lai Y, Cheng H, Gao Z, Zhang S, Chang X. Stress-strain relationships and nonlinear Mohr strength criteria of frozen sandy clay. Chin J Rock Mech Eng. 2007;50(1):45–53 **(in Chinese)**.

Lee H, Ong SH, Azeemuddin M, Goodman H. A wellbore stability model for formations with anisotropic rock strengths. J Pet Sci

Eng. 2012;96–97(19):109–19. https://doi.org/10.1016/j.petrol.2012.08.010.

Liu M, Jin Y, Lu Y, Chen M, Hou B, Chen W, Wen X, Yu X. A wellbore stability model for a deviated well in a transversely isotropic formation considering poroelastic effects. Rock Mech Rock En. 2006;49(9):1–16. https://doi.org/10.1007/s00603-016-1019-8.

Liu XJ, Liu K, Gou S, Liang L, Luo C, Guo Q. Water-soluble acrylamide sulfonate copolymer for inhibiting shale hydration. Ind Eng Chem Res. 2014;53(8):2903–10. https://doi.org/10.1021/ie403956d.

Liu XJ, Liu H, Luo PY, Liang DC, Huang JJ. Research on effect of drilling fluid on Kuqa shale strength behavior and its application. Chin J Rock Mech Eng. 2009;28(s2):3920–5 (in Chinese).

Rahman MK, Naseby D, Rahman SS. Borehole collapse analysis incorporating time-dependent pore pressure due to mud penetration in shales. J Pet Sci Eng. 2000;28(1):13–311. https://doi.org/10.1016/S0920-4105(00)00064-4.

Riley M, Young S, Stamatakis E, Steve Y, Katerine P H, Guido D S, Lou J. Wellbore stability in unconventional shales-the design of a nano-particle fluid. SPE Oil and Gas India Conference and Exhibition, 28–30 March, Mumbai, India; 2012. https://doi.org/10.2118/153729-MS

Roshan H, Rahman SS. A fully coupled chemo-poroelastic analysis of pore pressure and stress distribution around a wellbore in water active rocks. Rock Mech Rock Eng. 2011;44(2):199–21010. https://doi.org/10.1007/s00603-010-0104-7.

Salehi S, Hareland G, Nygaard R. Numerical simulations of wellbore stability in underbalanced-drilling wells. J Pet Sci Eng. 2010;72(3):229–35. https://doi.org/10.1016/j.petrol.2010.03.022.

Sayers CM, Nagy Z, Adachi J, Singh V, Tagbor K, Hooyman P. Determination of in-situ stress and rock strength using borehole acoustic data. SEG Tech Prog Expand Abstr. 2009;28(1):3505–9. https://doi.org/10.1190/1.3255591.

Takahashi T. Rock physics model for interpreting the compressive strength—seismic velocity relation of sedimentary rocks. ISRM regional symposium-7th Asian Rock Mechanics Symposium, 15–19 October, Seoul, Korea; 2012.

Tianshou M, Chen P. Study of meso-damage characteristics of shale hydration based on CT scanning technology. Pet Explor

Dev. 2014;41(2):249–56. https://doi.org/10.1016/S1876-3804(14)60029-X.

Wang BY, Deng JG, Zhou LZ, Lu W. Applied research of collapse cycle of shale in wellbore using a coupled physico-chemical model. Acta Pet Sin. 2006;27(3):130–2 (in Chinese).

Weger RJ, Eberli GP, Baechle GT, Massaferro JL, Sun YF. Quantification of pore structure and its effect on sonic velocity and permeability in carbonates. AAPG Bull. 2009;93(10):1297–317. https://doi.org/10.1306/05270909001.

Wilson MJ, Wilson L. Clay mineralogy and shale instability: an alternative conceptual analysis. Clay Miner. 2014;49(2):127–45. https://doi.org/10.1180/claymin.2014.049.2.01.

Xia HW, Moore ID. Estimation of maximum mud pressure in purely cohesive material during directional drilling. Geomech Geoeng. 2006;1(1):3–11. https://doi.org/10.1080/17486020600604024.

Xu JZ, Zhai C, Ranjith PG, Sun Y, Qin L. Petrological and ultrasonic velocity changes of coals caused by thermal cycling of liquid carbon dioxide in coalbed methane recovery. Fuel. 2019;249:15–26. https://doi.org/10.1016/j.fuel.2019.03.089.

Xu JZ, Zhai C, Liu S, Qin L, Wu S. Pore variation of three different metamorphic coals by multiple freezing-thawing cycles of liquid CO_2 injection for coalbed methane recovery. Fuel. 2017;208:41–51. https://doi.org/10.1016/j.fuel.2017.07.006.

Zhang L, Cao P, Radha KC. Evaluation of rock strength criteria for wellbore stability analysis. Int J Rock Mech Min Sci. 2010;47(8):1304–16. https://doi.org/10.1016/j.ijrmms.2010.09.001.

Zhong H, Qiu Z, Zhang D, Tang Z, Huang W, Wang W. Inhibiting shale hydration and dispersion with amine-terminated polyamidoamine dendrimers. J Nat Gas Sci Eng. 2016;28:52–60. https://doi.org/10.1016/j.jngse.2015.11.029.

Zhu J, Yang Z, Li X, Wang N, Jia M. Evaluation of different microwave heating parameters on the pore structure of oil shale samples. Energy Sci Eng. 2018;6:797–809. https://doi.org/10.1002/ese3.253.

Zou Y, Li JC, Laloui L, Zhao J. Analytical time-domain solution of plane wave propagation across a visco-elastic rock joint. Rock Mech Rock Eng. 2017;50(10):2731–47. https://doi.org/10.1007/s00603-017-1246-7.